scientific reports

Check for updates

OPEN

Electrochemical aptasensor for 2-amino-2-thiazoline-4-carboxylic acid (ATCA), a metabolite for cyanide poisoning

Hairunnisa Mohd Anas Khan[1], Nor Azah Yusof[1,2]✉, Shahrul Ainliah Alang Ahmad[1], Choo Yee Yu[3], Nurul Hanun Ahmad Raston[4] & Siti Fatimah Abd Rahman[5]✉

An alternative biomarker for assessing the cyanide levels in postmortem materials is crucial for investigating acute cyanide intoxication. Herein, an aptamer–ligand biorecognition system with high specificity was developed to detect acute cyanide poisoning via its secondary metabolite, 2-amino-2-thiazoline-4-carboxylic acid (ATCA). Potential aptamers were screened from a random library of 66-base single-stranded DNA using GO-SELEX, with individual aptamers being identified through single-stranded DNA sequencing. Molecular docking was employed to predict the affinity of these aptamers toward ATCA and selected counter-targets; these predictions were confirmed using thermodynamic analysis with an isothermal titration calorimeter. Owing to its label-free biomolecular binding interactions, Apt46 exhibited the highest affinity against ATCA and notable selectivity against structurally similar counter-targets. Thus, an amino-tagged Apt46 binding aptamer was attached to a carbon electrode modified with EDC–NHS-activated graphene oxide. The binding of Apt46 to ATCA was quantified by measuring current changes using differential pulse voltammetry. The aptasensor achieved a detection limit of 0.05 µg/mL and demonstrated suitability for detecting ATCA across various biological matrices, with the high recovery percentages ranging from 92.29 to 114.22%. Overall, the proposed ATCA aptasensor is promising for identifying ATCA metabolites in cases of acute cyanide exposure.

Keywords Cyanide, Electrochemical sensor, ATCA, Graphene oxide, Metabolite, Aptamer

In medicolegal investigations of cyanide poisoning, accurate and reliable cyanide concentrations are rarely achieved. The half-life of cyanide and its primary metabolite, thiocyanate, increase under chronic exposures[1–5], and lead to the depletion of sulfur donors[5]. The diminished sulfur donors impede the thiocyanate detoxification process, resulting in an elevated cyanide levels, and enzymatic activity that remains active after prolonged exposure[6,7]. Conversely, the duration of acute cyanide exposure was considerably shorter, preventing the detection of the toxic parent compound. Despite acute or chronic exposure, the detection of cyanide is challenging because of its volatile and nucleophilic nature[8]. Therefore, most studies have focused on thiocyanate because of its longer half-life[9,10]. However, the notable variability of thiocyanate in preexisting biological specimens necessitates the consideration of a stable metabolite, such as 2-amino-2-thiazoline-4-carboxylic acid (ATCA), as a potential alternative biomarker for cyanide determination, even in the absence of the parent compound[11,12].

ATCA, whose concentration is directly correlated with that of the parent molecule undergoing metabolism, remained stable for several months when stored in a freezer[13]. The direct correlation between ATCA and cyanide may help minimize the limiting factors associated with the parent compound, such as concentration fluctuations depending on storage conditions (time and temperature) and contamination by cyanogenic bacteria. In postmortem examinations, carcasses may be exposed to environmental cyanide absorption and diffusion during

[1]Department of Chemistry, Faculty of Science, Universiti Putra Malaysia, 43400 Serdang, Selangor, Malaysia. [2]Institute of Nanoscience and Nanotechnology (ION2), Universiti Putra Malaysia, 43400 Serdang, Selangor, Malaysia. [3]Institute of Bioscience, Universiti Putra Malaysia, 43400 Serdang, Selangor, Malaysia. [4]Department of Biological Sciences and Biotechnology, Faculty of Science and Technology, Universiti Kebangsaan Malaysia, 43600 Bangi, Selangor, Malaysia. [5]School of Electrical and Electronic Engineering, Engineering Campus, Universiti Sains Malaysia, 14300 Nibong Tebal, Pulau Pinang, Malaysia. ✉email: azahy@upm.edu.my; fatimahrahman@usm.my

sample collection and separation[14], resulting in variations in the total cyanide concentration[15]. These factors contributing to variations in the cyanide concentration may lead to false-positive or false-negative conclusions[13].

Therefore, the use of ATCA as a biomarker can minimize uncertainties and confirm the presence of cyanide[16], especially in poisoning cases in which the decomposition of cadavers and the closure of detectability windows may compromise the reliability of the cyanide concentration for toxicity determination in the involved specimens[17]. Although the forensic scientific community has not yet embraced the use of alternative biomarkers, such as thiocyanate, ATCA, and cyanide–protein adducts, the ATCA metabolite may serve as evidence for verifying cyanide intoxication[5].

Cyanide is distributed in red blood cells, serum, and plasma[13]. Therefore, Jackson and Logue[43] developed a portable and efficient diagnostic sensor based on fluorescent detection. This sensor has been thoroughly tested and proven to have a 100% accuracy rate in detecting blood cyanide in a rabbit model[18]. However, ongoing debates have raised concerns about the stability of cyanide in postmortem samples[19]. Elevated blood cyanide levels were observed in the blood of victims who had been burned after death, as reported in homicide cases[15]. The instability of cyanide complicates the determination of blood cyanide levels and exposure extent[17].

Further research into the applicability of ATCA in medicolegal investigations of cyanide poisoning is required because no current forensic toxicology test has been used to confirm the correct amount of cyanide in poisoning cases[13]. Consequently, this study introduces an aptamer with high selectivity and specificity for ATCA. The aptamer was selected as the receptor because, unlike antibodies, it is extremely stable across a broad temperature range and can revert to its original form even after several selection cycles of denaturation followed by renaturation[20]. In addition, aptamers are more feasible to produce than antibodies because they are chemically synthesized, whereas antibodies require colony screening using mammalian cell culture, leading to variations from batch to batch[21]. Furthermore, synthetic aptamers can be chemically modified to enhance their stability and make them resistant to nucleases[22,23]. Moreover, unlike highly immunogenic antibodies, aptamers do not provoke the human immune response and are thus not perceived as foreign materials by the human immune system[24]. Aptamers can recognize various targets including ions and small molecules that cannot be recognized by antibodies; thus, aptamers have wider applications as biosensors than antibodies[23].

Herein, we present an unexplored strategy for detecting cyanide poisoning by combining the merits of graphene oxide (GO) as immobilization matrixes and ATCA as a specific biomarker on a disposable screen-printed carbon electrode (SPCE)-based aptasensor. In addition to the high surface area of this 2-dimensional nanomaterial, GO possesses an advantage for the attachment of biological recognition elements owing to its versatile oxygen functional groups. For this purpose, the aptamer was screened through GO-SELEX from a single-stranded DNA random library and subsequently functionalized onto GO-modified SPCE to develop a voltammetric aptasensor. In clinical and forensic diagnostics, laboratory testing entails initial screening, followed by a confirmatory testing[25]. The proposed ATCA aptasensor can enhance the cyanide detection accuracy by reducing the false-positive and false-negative results in cases of cyanide intoxication. Stable biomarkers are crucial for detecting cyanide, as opposed to cyanide itself[16]. Notably, this simple and cost-effective method is efficient for screening ATCA in real sample applications, including blood, serum, and urine, without the need for advanced equipment or user expertise in forensic analysis.

Results and discussion

Aptamer selection by GO-SELEX

A high-throughput screening of aptamers with strong binding and selectivity for ATCA was conducted using a random library containing 438933.3 ng of ssDNA. Graphene oxide (GO) was used as a ssDNA carrier for the iterative selection. Before selection, both aptamers and GO underwent mass ratio optimization to determine the appropriate volume for the random library and sub-library incubation[26], as shown in Fig. 1a. The ideal mass ratio of GO to single-stranded DNA (ssDNA) was identified from the distinct binding kinetics seen with varying lengths of ssDNA and GO[26]. The random library consisted of n = 30 random nucleobases with 18-nt for both forward and reverse primers. Therefore, optimizing the mass ratio of GO/ssDNA was crucial to ensure the 66-nt ssDNA was completely adsorbed on the GO. The optimum mass ratio was determined from the fluorescent intensity of different mass ratios of GO/ssDNA. The fluorescent intensity decreased from 1567 to 38 dfu as the mass ratio increased from 0:1 to 25:1. Hence, the optimum GO volume for 1 µL of ssDNA was 25 µL.

The aptamer selection cycle started with the incubation of the 1 µL of ssDNA library with 25 µL of GO, followed by the incubation with a group of counter targets to minimize the aptamer candidates. Subsequently, the random aptamers unbound to counter targets were incubated with ATCA. The aptamers that were selective to the counter targets were discarded after centrifugation by removing the supernatant. After incubation with both targets and counter targets, the purified pool of ssDNA concentration was analyzed using a nanodrop bio spectrometer. The ssDNA was amplified, forming dsDNA, and after dsDNA purification, the dsDNA concentration was analyzed via a nanodrop bio spectrometer. The dsDNA was denatured by Urea-PAGE analysis to regenerate the ssDNA for the subsequent round of selection. The concentration of purified ssDNA after Urea–PAGE was analyzed using a nanodrop bio spectrometer, and the volume of the purified ssDNA was used to determine the ssDNA amount (ng). The same steps were repeated with the pooled ssDNA before PCR reached saturation state. In this study, the percentage of ssDNA recovery decreased after the sixth round of aptamer selection. Figure 1b shows the pooled ssDNA recovery percentage obtained from the seventh round of aptamer selection. The seventh-round aptamer selection reached saturation, in which the pooled ssDNA recovery was lower (95.6%) than in the previous round (96.4%). Hence, the ssDNA from the sixth round was amplified and sequenced for DNA cloning.

Twenty colonies were selected for DNA extraction and amplification. Amplicons were analyzed using gel electrophoresis. The 17 visible DNA bands were selected and subcultured into individual broths. Plasmid DNA

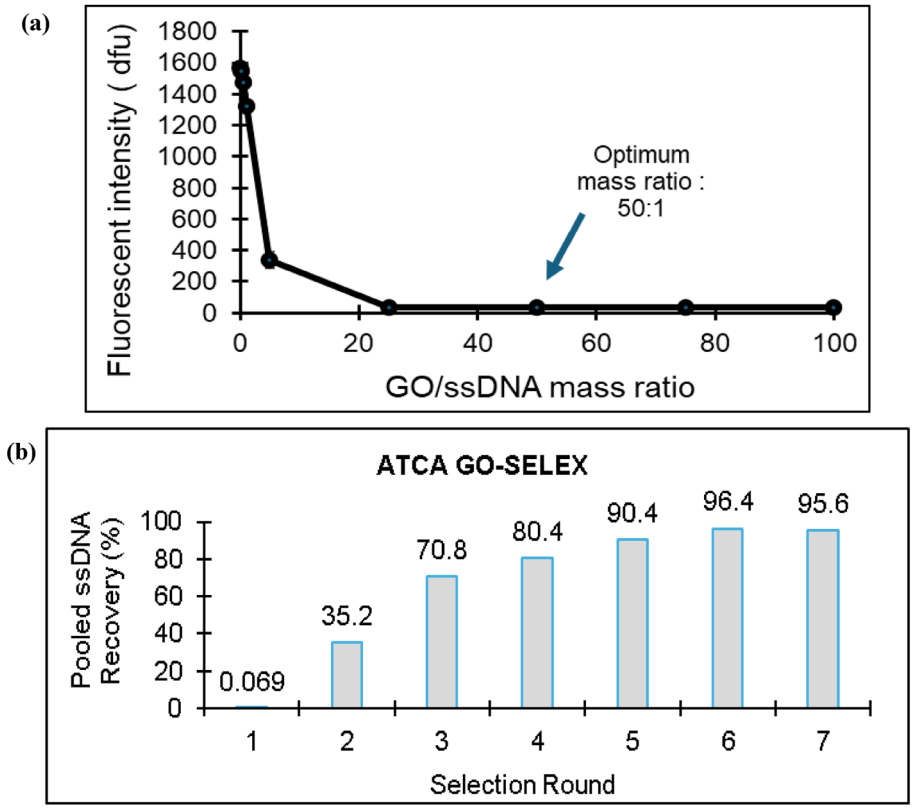

Fig.1. (**a**) Round selections of ssDNA aptamers for ATCA via GO-SELEX. (**b**) GO/ssDNA mass ratio fluorescent intensity (dfu).

from the colonies was extracted and sent for sequencing. Sequence candidates were analyzed for M-fold free energies and grouped into respective phylogenetic groups. A molecular docking analysis was performed for all aptamer candidates with the target ATCA. The two aptamers with the highest binding affinity were Apt20 and Apt46. These aptamers were selected for biomolecular-binding interaction characterization using isothermal titration calorimetry (ITC). The selectivity of the two selected aptamers was further assessed by molecular docking with the counter targets. According to binding affinity in molecular docking, both aptamers showed lower affinity for the counter targets. Figure 2a illustrates the molecular docking binding affinities of Apt20 and Apt46 to ATCA and the counter targets. Figure 2b shows the Apt20 (ΔG: −7.87 kcal/mol) and Apt46 (ΔG: −10.78 kcal/mol) M-fold structures.

The ITC is a label-free method that measures the heat released or adsorbed from the direct interaction between the aptamer and the ligand[27]. This instrument allows precise measurements of the disassociation constant (Kd), binding stoichiometry, and thermodynamic parameters of the interactions between two molecules[28]. In this analysis, the ATCA was titrated with Apt20 and Apt46. According to the thermogram displayed in Fig. 2c,d, both binding aptamers exhibited favorable binding interactions[27]. This is supported by the observed change in enthalpy, $\Delta H = -100$ kJ/mol. When comparing the disassociation constant (Kd) values, it was found that Apt46 (Kd: 5.02×10^{-9} M) had a lower value than Apt20 (Kd: 3.87×10^{-5} M). This indicates that Apt46 has a higher affinity for ATCA than Apt20. Thus, Apt46 was selected for further use in ATCA aptasensor development. Blank samples represent interactions between the phosphate-buffered saline solution and Apt20 and Apt46.

Characterization of ATCA aptasensor

The ATCA aptasensor utilized the aptamer sequence Apt46, which was labeled with an amino tag (5′/5AmMC6/CGT ACG GAA TTC GCT AGC CAA CGC TAG TGT GGT GGA TTA ACG AGT ACC CAC GTG GAG CTC GGA TCC-3′). This specific sequence demonstrated the highest selectivity and affinity for the target. The functionalization of Apt46 was carried out on SPCE.

Prior to that, the surface of the SPCE was modified with GO activated with EDC – NHS crosslinker. GO has functional groups with oxygen on its surface, resulting in the reduction of Π–Π stacking and deformation of the lattice structure that allows GO to interact with solvents by forming hydrogen bonds between the hydroxyl group on the GO sheet and any compounds present within the solvents[29]. Exploiting the existence of oxygen functional groups (= O, – OH, – O –, and – COOH) on the bilateral side of the sheets, including the borders of the plane[30], it readily interacts with EDC – NHS, as illustrated in Fig. 3. In this coupling reaction, EDC reacts with the carboxyl group of GO to form an unstable, reactive O-acylisourea ester. Sulfo-NHS reacts with the labile acylisourea ester to produce a slightly stable amine-reactive NHS ester[31]. When the aptamer is immobilized onto

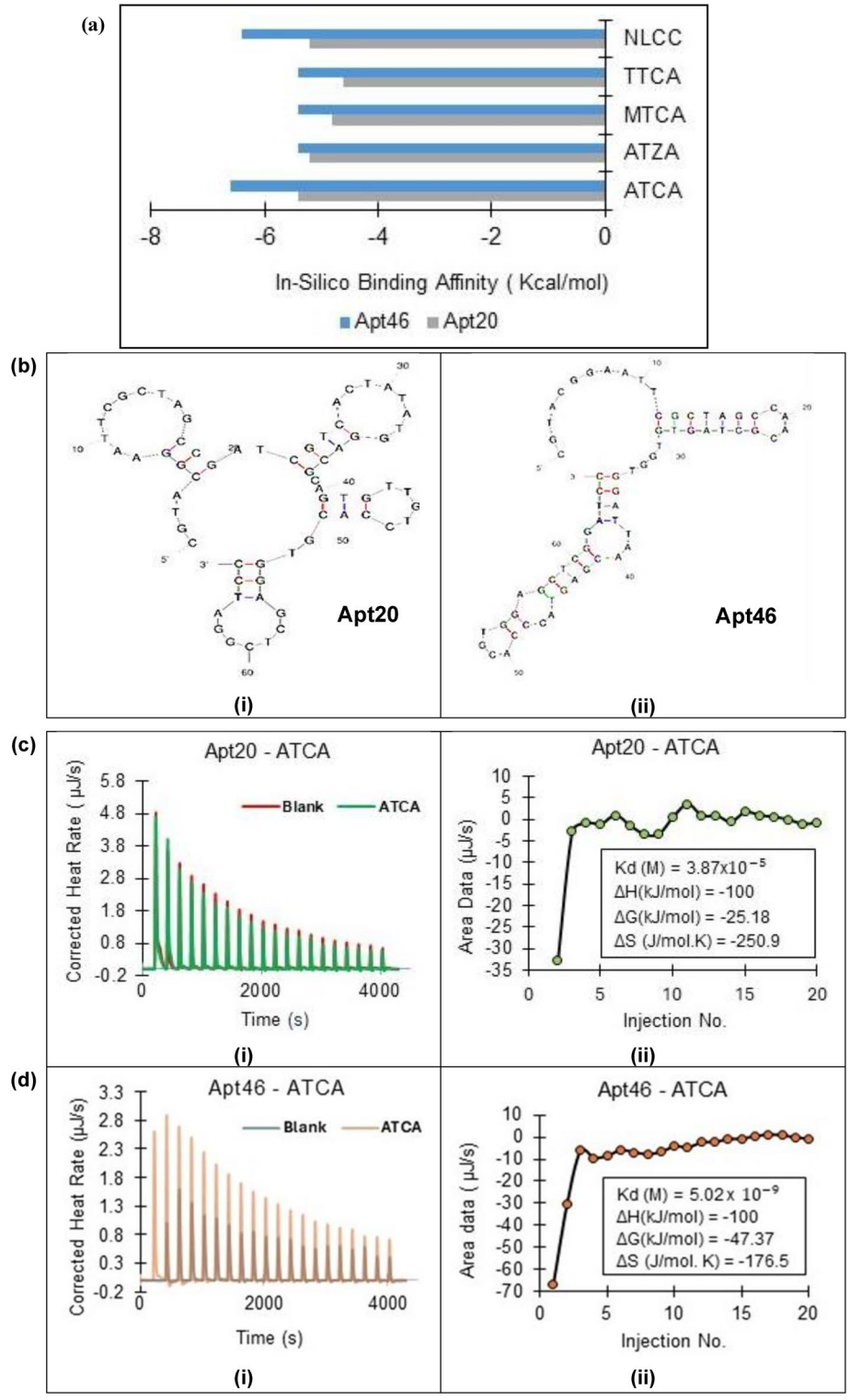

Fig.2. (**a**) In-silico binding affinity (kcal/mol) of APT20 and APT46 for various targets. (**b**) M-fold structures for (i) APT20 and (ii) Apt46. (**c**) Isothermal titration calorimetry (ITC) measurements of (i) Apt20 binding interaction with ATCA and blank (no metabolite as a control), and (ii) Apt20-ATCA using injection method. (**d**) ITC measurements of (i) Apt46 binding interactions with ATCA and blank, and (ii) Apt46-ATCA using injection method.

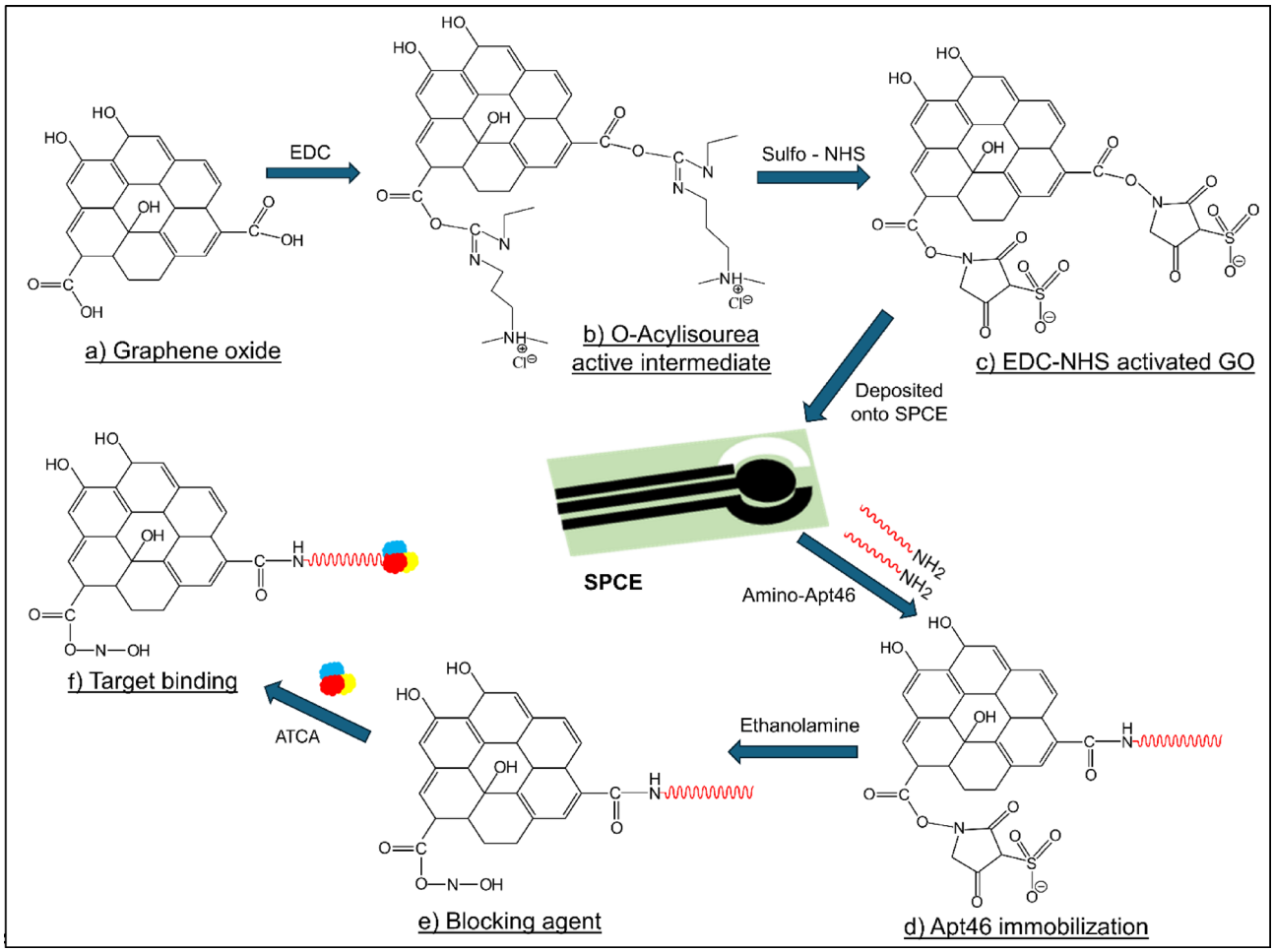

Fig.3. Scheme of the functionalization of graphene oxide (GO) with ssDNA: (**a**) surface chemistries of the GO sheet, including functional groups (=O, – OH, – O –, and – COOH), (**b**) formation of an O-acylisourea active intermediate via the 1-ethyl-3-(3-dimethylaminopropyl) carbodiimide (EDC) crosslinker, (**c**) surface stabilization of EDC–NHS/GO through the addition of sulfo–NHS, (**d**) immobilization of Amino-Apt46 on the EDC–NHS/GO/SPCE modified surface, (**e**) blocking of the unreacted active sites using ethanolamine, and (**f**) detection of the target ATCA on the immobilized electrode surface.

the SPCE, Apt46 reacts with the amine-reactive NHS ester. This approach successfully linked the carboxyl group of GO with the amino-labeled Apt46 using the EDC–NHS crosslinker. The assay's subsequent steps inhibited nonspecific binding by blocking with ethanolamine. After ATCA incubation, the immobilized Apt46 captures the target analyte. The Apt46–ATCA complex conformation facilitates electron transport between the redox probe and the bulk solution.

GO has been utilized as a DNA carrier in the GO-SELEX analysis. GO was preferred for aptamer functionalization due to its ability to interact with ssDNA instead of dsDNA. The ssDNA is a non-helical structure, while the dsDNA has a double helix structure that hinders direct interaction between graphene oxide and nucleobases[32,33]. The SPCE modified with GO activated EDC–NHS was characterized using FESEM/EDX analysis, as illustrated in Fig. 4. The GO-modified electrode exhibited a large sheet-like morphology with crumpled features, in contrast to the image of the bare SPCE with a rough surface structure, thereby confirming the presence of EDC–NHS/GO. Additionally, EDX analysis revealed a predominant peak corresponding to carbon in the bare SPCE, whereas GO/SPCE showed a dominant oxygen peak, confirming the successful attachment of GO to the SPCE surface. The weight percentage of oxygen in the GO-modified electrode was approximately 7% higher than in the unmodified SPCE, primarily attributed to the formation of oxygen-containing functional groups via GO sheet activation with EDC–NHS. In the EDC–NHS coupling reaction, EDC reacts with carboxyl groups on the GO surface to form a partially unstable acylisourea ester. Subsequently, sulfo-NHS was combined with the ester to form a partially stable NHS ester capable of reacting with amines. The NHS ester was then reacted with the amino-labeled aptamer to form a stable amide bond, as illustrated in Fig. 3.

The SPCE surface modification of the aptasensor was examined using cyclic voltammetry (CV), as depicted in Fig. 5a. CV analysis (scan rate:100 mVs^{-1}) was performed for each layer of electrode surface modification from the bare electrode to the target ATCA immobilization. The bare SPCE exhibited the minimum changes in peak current due to the disabled access of the redox probe $[Fe(CN)_6]^{4-/3-}$ to the electrode surface. After modification with EDC – NHS-activated GO, the peak current increased as the neutrally charged NHS allowed the passage of

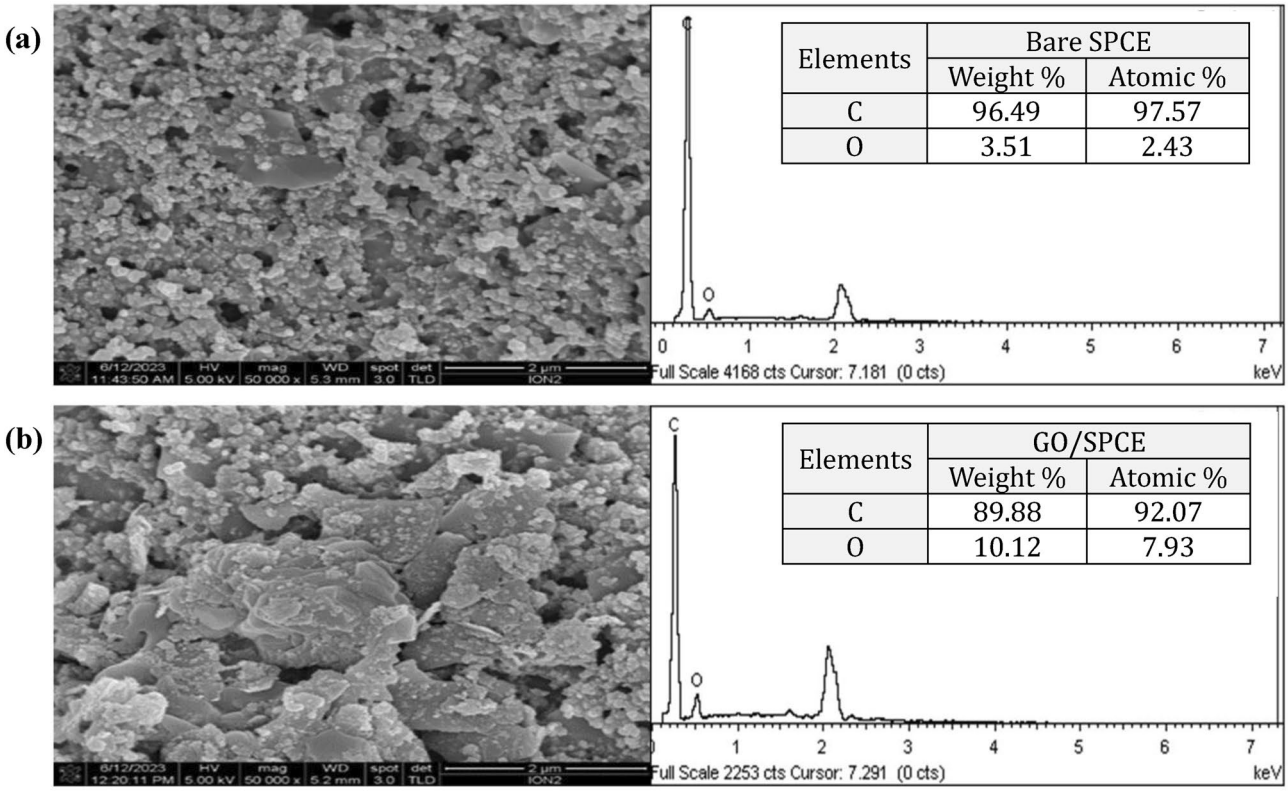

Fig.4. Morphological and elemental analysis using FESEM/EDX for (**a**) bare SPCE and (**b**) GO-modified SPCE at scale of 200 nm.

the redox probe to the electrode surface. Subsequently, after immobilization of the aptamer, a substantial decrease in peak current was observed because of an increase in the charge transfer resistance caused by the negatively charged Apt46 backbone, which obstructs the negative redox probe from reaching the active site for electron transfer. The peak current slightly increased after the ethanolamine blocking step because of the blockage of the negatively charged and unreacted carboxyl group, which allowed the negative redox probe to access the electrode active site. After incubation with ATCA, the aptamer bound to the small-molecule analyte and formed a hairpin structure that increased the electroactive surface area of the redox probe[34,35].

The Apt46 aptasensor was also developed by electrochemical impedance spectroscopy (EIS), as shown in Fig. 5b. In this characterization, the magnitude of the electron transfer resistance (Rct) was determined from the diameter of the Nyquist plot semicircle. Before the modification with activated GO, the diameter of the bare SPCE semicircle was large because of the high electron transfer resistance at the active site of the working electrode. After the electrode was modified with activated GO, the electron transfer resistance was dramatically decreased because of the activation of the carboxyl group on the surface of the GO by EDC – NHS, which induced the alleviation of electrostatic hindrance from the electronegative carboxyl group[35]. Besides, the decrease in Rct could be attributed to the replacement of the carboxyl group with the neutral NHS ester, which allowed the transfer of a negative probe $[Fe(CN)_6]^{4-/3-}$ on the surface of the electrode[34].

Subsequently, when the Apt46-binding aptamer was immobilized on the electrode surface, Rct increased because of the presence of negative charges on the aptamer phosphate backbone, which induced repulsion toward the negatively charged redox probe. Following the blocking of the unreacted carboxyl group with ethanolamine, the negatively charged carboxyl group on the surface of the electrode reduced the resistance of the negatively charged electrode probe from reaching the electrode surface. After incubation with the target ATCA, the value of Rct was further reduced. The reduction in electron transfer resistance was presumed to be due to the aptamer enclosing the small-molecule ATCA to form a hairpin structure[36], as depicted in Fig. 5d, and opening the access for the redox probe to the electrode surface.

Randles circuit fittings were conducted for each alteration layer to further examine the actual charge transfer resistance. Bare SPCE showed high impedance in EIS (2.6×10^3 Ω) due to the low conductivity of the carbon-based material. After modification with GO, the charge transfer resistance decreased to 24.7 Ω. Upon modification with the Apt46-binding aptamer, the charge transfer resistance increased to 40.4 Ω and shifted to 32.1 Ω after the immobilization of ethanolamine. The final step modification with target ATCA reduced Rct to 27.0 Ω, as listed in Table 1. The Nyquist plot overlay for the surface modification is shown in the inset of Fig. 5c.

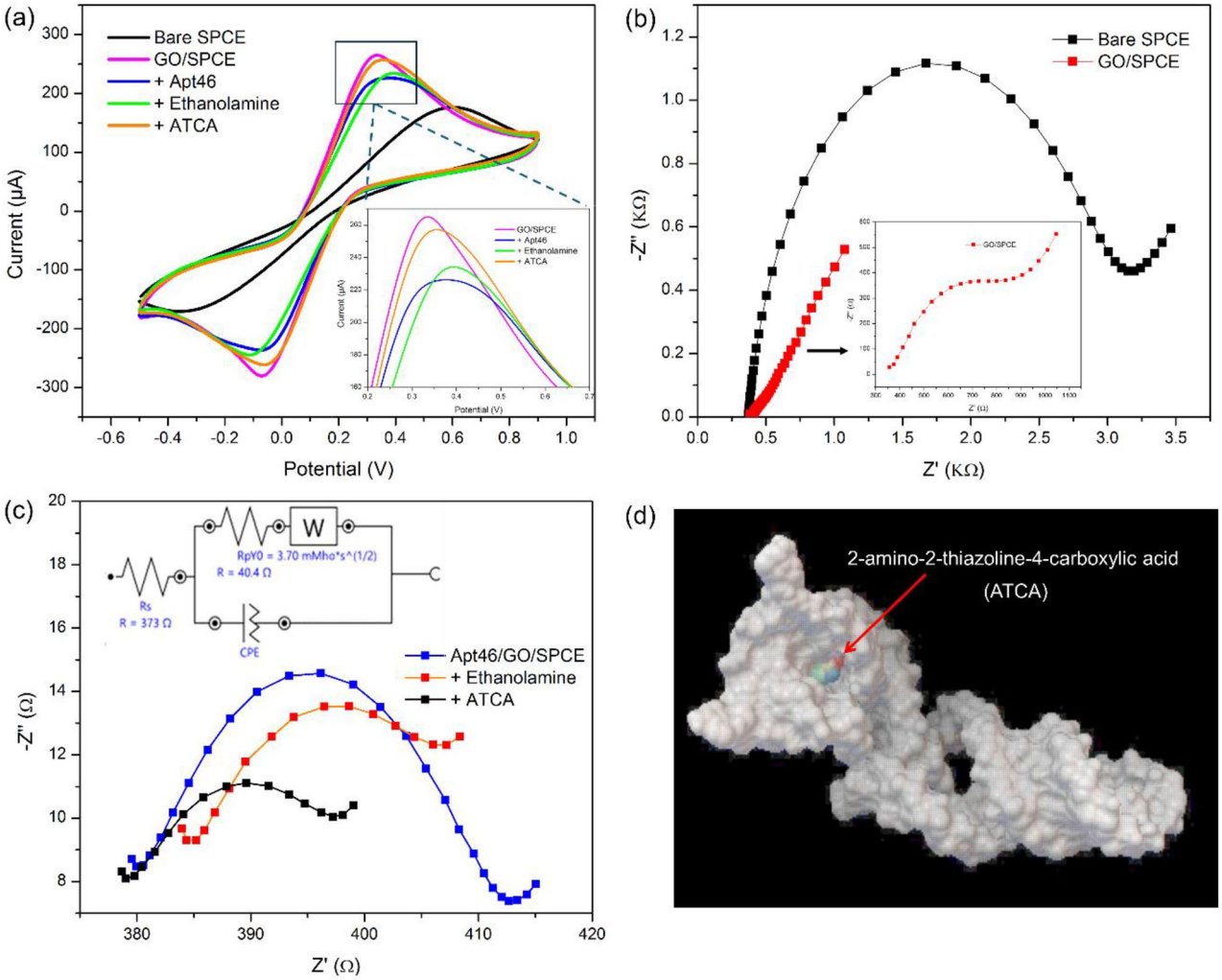

Fig.5. (**a**) Cyclic voltammogram of bare SPCE and different modified electrodes. (**b**)-(**c**) Nyquist plots of the stepwise fabrication process of Apt46-based GO-modified SPCE for ATCA detection in 1 mM $[Fe(CN)_6]^{4-/3-}$ solution containing 1 × binding buffer (1 × BB), pH 7.6. The Apt46 and ATCA concentrations were 0.3 μM and 0.35 μg/mL, respectively (Inset is an equivalent Randles circuit: Rs = resistance between the working and reference electrodes, Zw = Warburg impedance, Cdl = double-layer capacitance, and Rct = charge-transfer resistance). (**d**) ATCA-Apt46 three-dimensional molecular docking conformation.

Electrode	Rs (Ω)	Rct (Ω)	CPE(μM)	Chi-squared(X^2)
Bare SPCE	372	2600	2.31	3.23×10^{-2}
GO/SPCE	379	24.7	52.8	5.93×10^{-6}
Apt46/GO/SPCE	373	40.4	10.9	6.95×10^{-4}
ET/Apt46/GO/SPCE	377	32.1	6.69	6.62×10^{-5}
ATCA/ET/Apt46/GO/SPCE	372	27.0	7.93	1.48×10^{-5}

Table 1. Randles circuit fittings. *Apt* aptamer, *CPE* constant phase element, *GO* graphene oxide, *ET* ethanolamine, *SPCE* screen printed carbon electrode.

Analytical performance of ATCA aptasensor

The development of the ATCA aptasensor was optimized by differential pulse voltammetry (DPV). The optimized parameters included the Apt46 ligand and ethanolamine concentrations, as well as aptamer, ethanolamine, and target ATCA incubation times (Fig. 6). The method was adapted from Aye and group[37]. The ATCA concentration was consistently set at 0.35 μg/mL throughout the optimization process. The optimization was performed with Apt46 concentration from 0.1 to 1.0 μM.

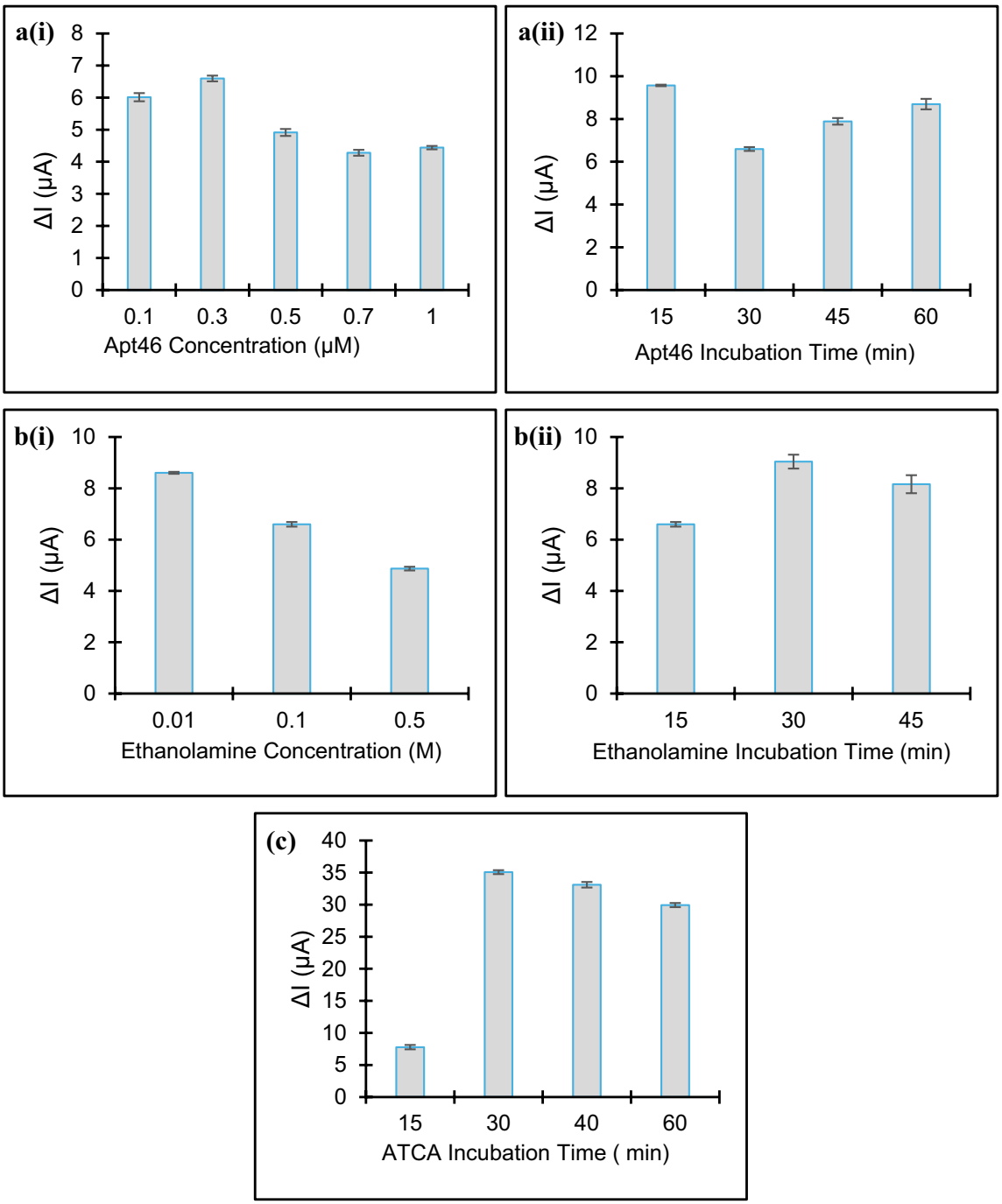

Fig.6. (**a**) Effect of Apt46 (i) concentration and (ii) incubation time; (**b**) Effect of Ethanolamine (i) concentration and (ii) incubation time; (**c**) Effect of ATCA incubation time.

The optimum Apt46 concentration was determined to be 0.3 μM, while 15 min was determined to be the best duration for aptamer incubation to the ligand. The electrode surface was rinsed with 100 μL of binding buffer (1 × BB) for every modification layer. The subsequent optimization was the concentration of the blocking agent, ethanolamine. The blocking agent was immobilized after aptamer modification to avoid nonspecific binding on the surface of the GO/SPCE, with other than the aptamer probe to increase the aptamer efficiency[38]. The optimized ethanolamine concentration and time for incubation were 0.01 M and 30 min, respectively. The ATCA incubation time was also optimized to determine the most effective duration for complete interaction between the aptamer and the analyte prior to DPV measurement.

A calibration plot was developed using the optimized parameters. The ATCA was added to the binding buffer (1 × BB) at concentrations ranging from 0.05 to 1.5 μg/mL. The changes in current (ΔI) response increased as the concentration of the spiked analyte increased, as depicted in Figs. 7a ,b. The aptamer characterisation using

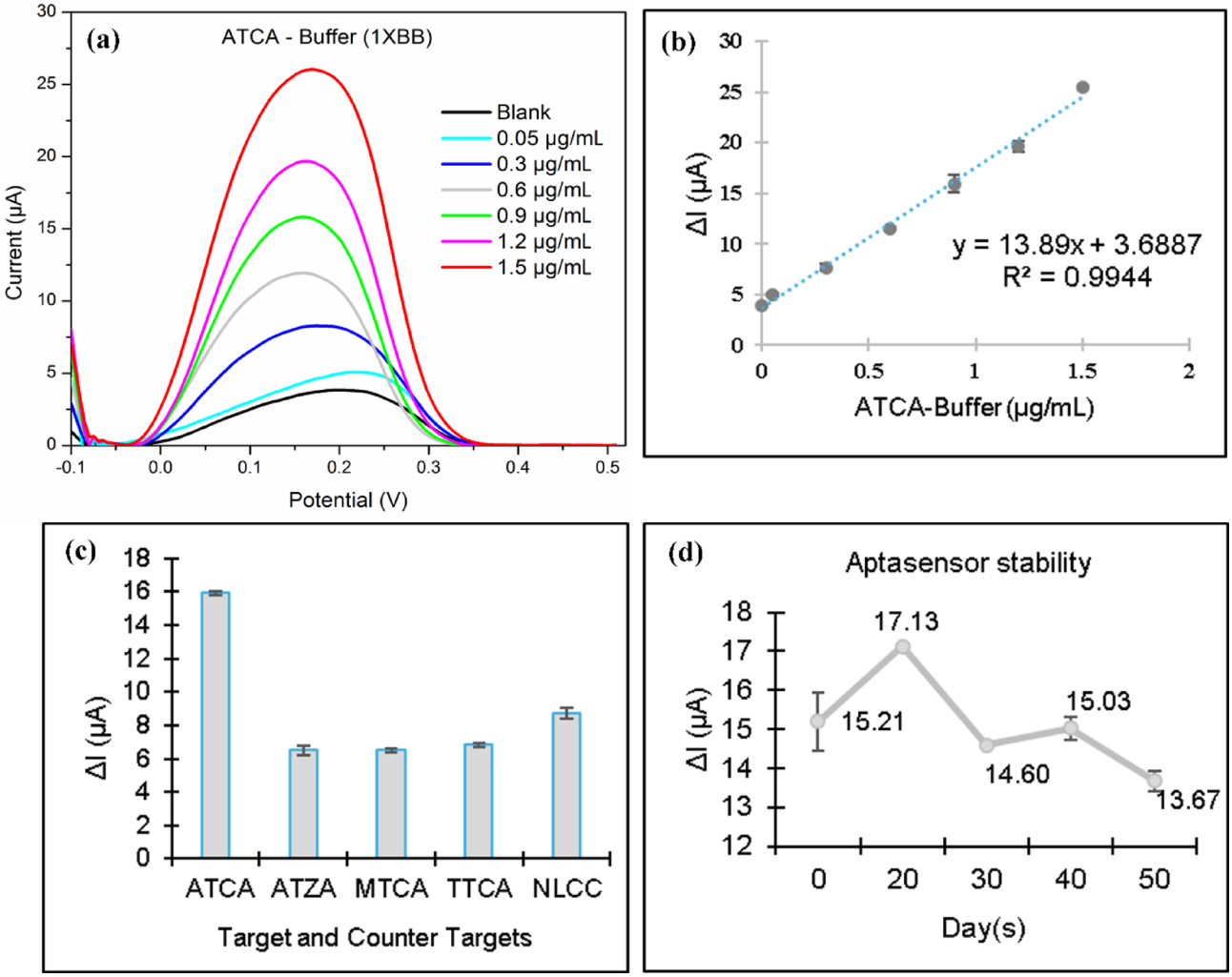

Fig.7. (**a**) DPV response of ATCA-Buffer (1 × BB). (**b**) The calibration curve of the current changes corresponding to the ATCA-Buffer concentration range of 0.05 to 1.5 µg/mL. (**c**) ATCA aptasensor cross-reactivity analysis against target and counter targets. (**d**) Apt46 DPV response stability standard deviation range.

CV and EIS confirmed that the current increased while the charge resistance decreased when the ATCA was immobilized on the modified electrode.

The performance of the ATCA aptasensor to discriminate its GO-SELEX counters targets was examined by performing a cross-reactivity analysis with 2-Aminothiazole-4-carboxylic acid (ATZA), 2-Methylthiazole-4-carboxylic acid (MTCA), (4R) -(-)-2-Thioxo-4-thiazolinecarboxylic acid (TTCA), and N-Carbamoyl—L- Cysteine (NLCC) as shown in Fig. 7c. Based on the findings, the ATCA aptasensor could recognize the same counter-targets used in the aptamer screening cycles. The DPV response towards the counter targets was consistent with the virtual binding affinity screening against both target and counter targets, as presented in Fig. 2a.

Furthermore, the stability of the ATCA aptasensor was analyzed in detail. Five sets of Apt46/GO/SPCE triplicate samples were prepared and monitored for 50 days, as shown in Fig. 7d. The samples were deposited on days 1, 20, 30, 40, and 50. Apt46/GO/SPCE was placed in a petri dish and sealed with parafilm. All the samples were stored at a temperature of 4 ℃ from day 1 to day 50. The stability of ATCA was conducted in the binding buffer matrix. The system remained stable for 50 days with a mean recovery of spiked ATCA (0.90 µg/mL) within ± 3SD as shown in Table 2.

Application of ATCA aptasensor in biological matrices

The applicability of the ATCA aptasensor to biological samples was evaluated by developing calibration plots for the individual matrices (Fig. 8), i.e., blood, serum, and urine, followed by conducting repeatability analysis. ATCA was spiked in different matrices and analyzed in triplicates (n = 3) on different days. Table 3 represents the DPV response recovery of the toxic level of ATCA (0.90 µg/mL). The percent recoveries were obtained from the ratio of the mean from inter-day responses against the DPV response of the mean of 0.9 µg/mL from the calibration curve. Based on the repeatability analysis, a good recovery percentage ranging from 92.29 to 114.22% was obtained. Moreover, the RSD values for the samples (n = 3) were below 5%.

Apt46 DPV response (n = 3) stability standard deviation (SD) range	
3SD	17.4520
2SD	16.7041
1SD	15.9562
Mean	15.2083
1SD	14.4603
2SD	13.7124
3SD	12.9645

Table 2. Stability of developed ATCA aptasensor.

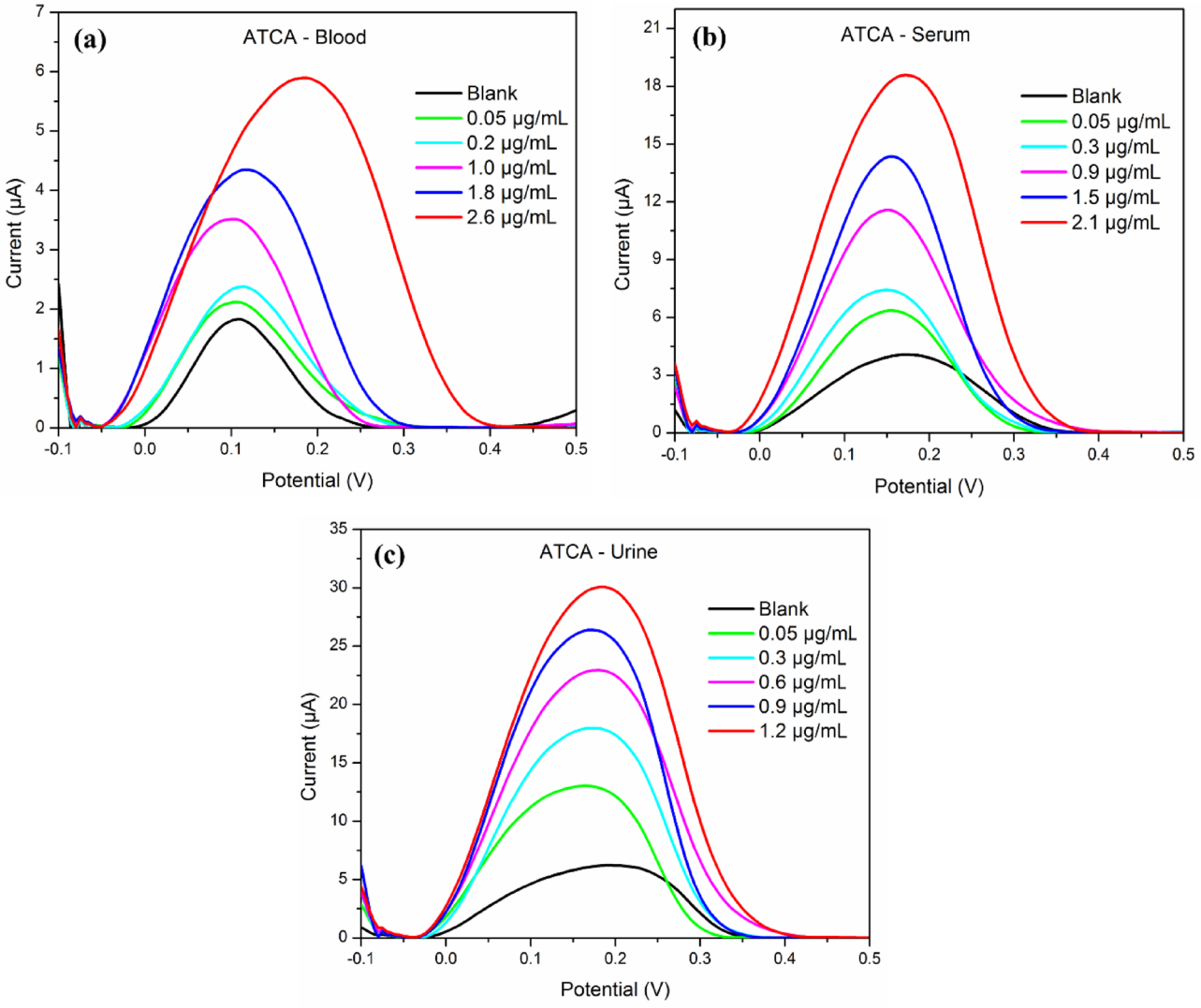

Fig.8. ATCA–DPV responses for (**a**) blood spiked, (**b**) urine spiked, and (**c**) serum spiked.

To date, analytical methods for detecting ATCA mainly use gas and liquid chromatography. In gas spectrometry-mass spectrometry (GCMS) analysis, the derivatization process is required because ATCA is a highly polar and non–volatile compound[39,40]. The derivatizing agent, MSTFA, reacts with the primary, secondary amine, and carboxylic acid moieties of ATCA. After derivatization, ATCA becomes more volatile and is readily injected into GCMS[39]. The polar ATCA compound is separated in liquid chromatography using a hydrophilic interaction chromatography column and identified using tandem mass spectrometry (LC/MS/MS). Derivatizing agents,

Spiked ATCA (0.90 µg/mL)	Coefficient of determination (R^2)	Days	Calibration standards (ΔI/µA)	Repeatability (ΔI/µA)	Recovery (%)	RSD (%) (n = 3)
Buffer	0.9944	1	15.91	15.31	96.22	2.3177
		2		16.46	103.45	2.5688
Urine	0.9901	1	26.89	28.39	105.57	2.1274
		2		25.85	96.13	1.6885
		3		26.94	100.16	0.7899
Serum	0.9946	1	11.85	10.94	92.29	1.0896
		2		12.83	108.28	1.7812
		3		13.54	114.22	3.0183
Blood	0.9971	1	3.4	3.23	95.00	2.8597
		2		3.77	110.88	3.4458
		3		3.40	100.00	1.2321

Table 3. ATCA aptasensor spike recovery in both buffer and biological matrices.

such as S–NIFE and DNS, are employed in liquid chromatography to purify post-mortem blood. It was noted that the interference reduced after cleaning up with S-NIFE, and the analyte peak shape improved[41]. GCMS and LCMS instrumental methods for ATCA analysis need a derivatizing process, making it costly, laborious, and require a longer analysis time[42,43]. The available ATCA analytical instrumental methods are listed in Table 4. The detection limit for this study is comparable to that of the previous research. The baseline level of ATCA in human blood was reported to be approximately 0.15 µg/mL[41].

Conclusion

This research focused on screening for an aptamer with the highest affinity for 2-amino-2-thiazoline-4-carboxylic acid (ATCA), the secondary metabolite of cyanide, using graphene-oxide SELEX. To estimate the specificity of the random aptamer for ATCA, a random ssDNA library was incubated with structurally similar counter-targets before the actual target to minimize nonspecific candidates. Among these counter-targets, 2-aminothiazole-4-carboxylic acid closely resembled ATCA but differed by having two double bonds in the ring structure, compared with the ATCA's single double bond. The binding aptamer Apt46 demonstrated higher specificity toward ATCA over Apt20, with the dissociation constants of $5.02 \times 10{-}^{9}$ M and $3.87 \times 10{-}^{5}$ M, respectively. Consequently, amino-labeled Apt46 was functionalized on the carbon electrode previously modified with an EDC–NHS linker to develop an ATCA aptasensor. This aptasensor demonstrated exceptional affinity for ATCA compared with selected counter-targets and remained stable for up to 50 days, with deviations in the current response being limited to ± 3SD. It could detect ATCA directly in various biological samples, including urine, serum, and whole

Biological specimen	Extraction method	Derivatizing agent (s)	Separation technique	Detection mode	LOD	Sample recovery	Ref
Urine	LLE	MSTFA	GC	MS	25 ng/mL		39
Human urine	MISBSE	–	RPLC	MS/MS	5 µg/L	–	46
Rat plasma and organ	SPE	–	RPLC	MS/MS	–	–	16
Rat plasma	SPE	–	RPLC	MS/MS	12 µg/L	–	47
Human post-mortem blood	SPE	–	HILIC	MS/MS	2.5 µg/L	81–89%	48
Human post-mortem blood	LLE	–	HILIC	MS/MS	0.43 µg/L	86–101%	41
Human post-mortem blood	LLE	DNS and S-NIFE	RPLC	MS/MS	1.5 ng/mL	91 -101%	41
Human post-mortem blood	SPE	–	HILIC	MS/MS	9 µg/L (LOQ)	88–96%	49
Blood	DMSPE	MSTFA	GC	MS	24 ng/mL		50
Human post-mortem blood	Direct	2,3-naphthalenedialdehyde (NDA) and taurine	PESI	MS/MS	43 ng/mL	–	51
Human blood	Direct	–	Aptasensor	DPV	0.05 µg/mL	95–110%	This work
Human serum	Direct	–	Aptasensor	DPV	0.05 µg/mL	92–114%	This work
Human urine	Direct	–	Aptasensor	DPV	0.05 µg/mL	92–100%	This work

Table 4. Methods for determination of ATCA. *DMSPE* dispersive micro solid phase extraction, *DNS* dansyl derivatization, *DPV* differential pulse voltammetry, *GC* gas chromatography, *HILIC* hydrophilic interaction chromatography (or hydrophilic interaction liquid chromatography, *LLE* liquid–liquid extraction, *LOD* limit of detection; *MISBSE* Molecularly imprinted stir bar sorption extraction, *MS* mass spectrometry, *MSTFA* N-Trimethylsilyl-N-methyl trifluoroacetamide, *PESI* probe electrospray ionization, *RPLC* reversed phase liquid chromatography, *S-NIFE* (S)-N-4-nitrophenoxycarbonyl) phenylalanine methoxyethyl ester, *SPE* solid phase extraction.

blood. Thus, this aptasensor can be used to detect the cyanide metabolite in investigations related to cyanide intoxication.

Methods

Materials and reagents

(4R)-(−)-2-Thioxo-4-thiazolinecarboxylic acid, 2-Aminothiazole-4-carboxylic acid, 2-Methylthiazole-4-carboxylic acid, acrylamide, ammonium persulfate, ampicillin, calcium chloride, ethanol, N-Carbamoyl-L-cysteine, trizma base, N′-Tetramethyl ethylenediamine (Temed), hydrochloric acid, phosphate buffered saline (PBS) tablet, and sodium acetate buffer solution (pH 5.2) were purchased from Sigma-Aldrich, USA. Formamide, potassium hexacyanoferrate (II) trihydrate were purchased from Merk, Malaysia. Graphene oxide in water suspension (4 mg/mL) was purchased from Graphenea, USA. Potassium chloride and sodium hydroxide were obtained from R&M Chemicals, India. Magnesium chloride and potassium ferricyanide were purchased from Bendosen, Malaysia. 10X Tris–Borate-EDTA (TBE) buffer (pH 8.3), PrimeWay plasmid DNA extraction kit, and agarose were purchased from 1st BASE Biochemicals, Malaysia. Glycogen Invitrogen™, O'RangeRuler 10 bp DNA ladder, TOPO® TA cloning® kit, and UltraPure™ 0.5 M EDTA (H 8.0) were obtained from Thermofisher Scientific, USA. GelPilot DNA loading dye was purchased from Qiagen, Malaysia. APTENS Screen Printed Sensors (Model SPE-RL3-05-P, Amperometric-Type 3 Channel WE (5 mm dia.)/RE/CE was purchased from Biogenes Technologies Sdn Bhd.

Optimization of GO/ssDNA

The ssDNA library used in this study consists of n = 30 random nucleobases with 18-nt for both forward and reverse primers. The optimal mass ratio of GO/ssDNA was determined because different lengths of ssDNA and GO showed dissimilar binding kinetics characteristics. Therefore, optimizing the mass ratio of GO/ssDNA is crucial to ensure the 66-nt ssDNA is completely adsorbed on the GO. GO solutions with different amounts were added to 10.5 uL of 10 µM 66-nt ssDNA labeled with 56-FAM (equivalent to 2 µg) (the 10 µM ssDNA was prepared in sterile deionized water). The binding buffer (1 × BB) was used as a solvent to determine the mass ratio GO/ssDNA. The mixture was gently mixed and incubated at room temperature with rotation for 1 h and centrifuged at 12,000 rpm for 15 min. The supernatants were collected for fluorescence intensity measurement using a Qubit R 2.0 Fluorometer.

In vitro selection of ATCA aptamers

The GO-SELEX procedure is adapted from N.H. Ahmad Raston et al.[44]. Heat shock analysis was performed by heating 200 pmol of the random library (5′-C GTA CGG AAT TCG CTA GC-(N30)-CA CGT GGA GCT CGG ATC C-3′) at 95 ℃ for 15 min and then cooling on ice flakes for 5 min on ice allowing the oligonucleotide to form the best structure. For every aptamer screening cycle, the denatured ssDNA was incubated on a rotator for 30 min with the ATCA counter targets; 2-Aminothiazole-4-carboxylic acid (ATZA), 2-Methylthiazole-4-carboxylic acid (MTCA), N-Carbamoyl—L- Cysteine (NLCC), and (4R) -(-)-2-Thioxo-4-thiazolinecarboxylic acid (TTCA) in the 1 × binding buffer (1 × BB) (100 mM NaCl, 20 mM Tris–HCl, 2 mM MgCl2, 5 mM KCl, 1 mM CaCl2, pH 7.6) to remove the ssDNA that have higher affinity for the counter targets. To remove the aptamer bound to the counter targets, 25 µL of 4 mg/mL GO was added (final volume 1 mL), and the incubation continued for 2 h.

The aptamer bound explicitly to the counter targets was separated by centrifugation at 1500 g rpm for 10 min, and the supernatant was discarded. The GO pellet left was added to the ATCA. The following 2 h of incubation aimed to allow the aptamer pools to form conformation with the target, and the binding complex was separated by centrifugation at 15000 g for 15 min. In this step, the supernatant was collected and re-centrifuged at the same setting as before to ensure the final supernatant was free from traces of GO. The GO-free supernatant proceeded with ethanol precipitation, and the ssDNA recovery was analyzed using a nanodrop spectrometer. The pooled ssDNA obtained was amplified via PCR using forward primer (5′-/56-FAM/CGTACGGAATTCGCTAGC-3′) and reversed primer (5′-(A20) /iSp18/ G GAT CCG AGC TCC ACG TG-3′). The ssDNA was recovered again by Urea-PAGE separation and purification. The denatured DNA was used as a random ssDNA pool for the following cycles and continued until the plateau was reached.

Cloning and sequencing of selected DNA

The ssDNA from the sixth round was amplified for DNA cloning using TOPO® TA cloning® Kit. The transformed cells (50 µL) were spread on the pre-warmed LB plates containing 50 µL Ampicillin and 40 µL of 40 mg/mL Xgal and incubated overnight. The white colonies were determined, picked using an inoculation loop, and spread on a new LB + Amp plate. Each colony picked from the incubated plates was streaked and incubated overnight. Only 20 colonies were randomly chosen for DNA extraction and underwent colony PCR analysis. The ssDNA was amplified using M13 Forward (−20) Primer and M13 Reverse Primer. The colony PCR products were analyzed using agarose gel electrophoresis, and the sample with a visible DNA band was prepared for plasmid DNA extraction analysis.

The plasmid DNA pellets were extracted using a Prime Way Plasmid Extraction Kit. The recovered Plasmid DNA concentrations were recorded using a biospectrometer and sent for sequencing. The sequencing results were analyzed using Applied Biosystems Sequence Scanner Software 2.0. The multiple sequence results were aligned using the Clustal Omega Program, and the aptamer was synthesized using the Mfold web server for nucleic acid folding and hybridization prediction. The folded DNA structure resulted in a circular plot (2D sequence) with a Gibbs free energy value in kcal/mol.

Molecular docking analysis

The molecular docking was performed via Autodock Vina Tool 1.5.6, MGL Tool 1.5.6, CADD 1.5.6, and Vision 1.5.6. This analysis was performed in Windows operating systems. The analytical procedure was adapted from the Simplified Learning Protocol by Biogenes Technologies Sdn Bhd. In addition, PyMOL tool was used for docking data analysis. The target (ATCA) and counter targets (ATZA, MTCA, NLCC, and TTCA) 3D conformers were downloaded from the PubChem website in sdf format and converted to pdb format using the Avogadro tool. The aptamers were obtained from the previous analysis and further analyzed for the docking analysis. The docking analysis aimed to reduce the number of potential aptamers. Initially, each aptamer was docked to the target to identify the two conformations with the highest affinity. This was followed by testing the selectivity conformation against the counter-targets.

Isothermal titration calorimetry (ITC) study

The virtual selection of aptamers was conducted using molecular docking analysis. Label free molecular binding interaction analysis was performed using an isothermal titration calorimeter to further study the aptamers. Specifically, two aptamers, Apt20 and Apt46, were titrated against the ATCA for affinity and specificity analysis. Blank samples were also tested for potential heat from buffer and ligand interaction. In the previous section, these counter-targets had already been docked against Apt20 and Apt46. The ligands (target and counter targets) and the macromolecule (aptamers) were prepared at 20 µM and 4 µM concentrations, respectively. The buffer used in this analysis was Phosphate Buffer Saline (PBS) solution, PH 7.6, with additional salt, MgCl2, to facilitate aptamers folding[45]. The salt concentration was similar to the GO-SELEX binding buffer, 2 mM $MgCl_2.6H_2O$.

Electrochemical detection of ATCA

The methodology in this research was adapted from Aye et al.[37]. The oxygen functional group-rich graphene oxide was immobilized onto the SPCE to improve the electrode's conductivity. The 10 mL of 400 µM EDC–NHS was added to 0.1 g of GO powder to form a crosslinker NHS ester to react with the primary amine group of the Apt46. The mixture was mixed and stirred for 4 h at room temperature, followed by 10 min of sonication. The activated EDC–NHS/GO was extracted by centrifuging at 10,000 rpm for 25 min. The resulting supernatant was discarded, and the excess EDC–NHS was washed away by rinsing it with deionized water (DIW). The activated solid GO was left to dry at 30 ℃ for 24 h.

A working suspension with a concentration of 0.5 mg/mL was prepared by adding 0.5 mg of the dried GO into 1 mL of DIW. The 7 µL of 0.5 mg/mL GO was dropped on the electrode and dried at 50 ℃ for 15 min. The excess GO was washed with 100 µL of binding buffer (1 × BB). The activated electrode was air-dried at room temperature. The dried SPCE and the bare SPCE were characterized via FESEM/EDX. The electrodes were further characterized by CV scanning rate at 0.01 – 0.1 V. Next, the SPCE was further characterized by depositing the subsequent layers of modification, i.e., 0.3 µM Apt46 followed by 0.35 µg/mL of ATCA. Every modification layer was washed with 100 µL 1 × BB and dried at room temperature. The SPCE surface was scanned at each level of deposition to observe the effects of modification. The amount of ATCA was taken from the toxic level of the ATCA. The redox probe used in this study was 5 mM $[Fe(CN)_6]^{4-/3-}$and 0.1 M KCl.

The electrochemical circuits for every level of modifications were analysed with EIS to perform the electrical circuit fitting for the surface modified SPCE model. The frequency (HZ) was set in the range of 0.01 – 1E + 05, and the amplitude (VRMS) was 0.05. The DPV method was used to optimize the modification of the electrode surface. The analytes were prepared in the GO-SELEX binding buffer, and Apt46 was prepared in sterilized-filtered DIW. The potential applied was in the range of −0.1 V to + 0.3 V with a pulse amplitude of 25 mV. The optimized parameters were Apt46 ligand concentration, ethanolamine concentration, aptamer incubation time, ethanolamine incubation time, and target-ATCA incubation time. The target and counter targets were spiked into the binding buffer and biological samples. The biological samples were human urine, serum, and whole blood. The recovery analysis was performed for two days in the binding buffer and three days in the biological samples. The stability analysis was conducted at a lethal dose of ATCA (0.90 µg/mL) in the binding buffer matrix. The electrode (Ethanolamine/Apt46/GO/SPCE) was prepared on the first day and the triplicate samples were kept in the fridge at 4 ℃ until use within 50 days.

Data availability

All data generated or analyzed during this study are included in this article.

Received: 7 April 2024; Accepted: 9 September 2024
Published online: 11 October 2024

References

1. Dirikolu, L. *et al.* The toxicokinetics of cyanide and mandelonitrile in the horse and their relevance to the mare reproductive loss syndrome. *Toxicol. Mech. Methods* **13**, 199–211 (2003).
2. Lanno, R. P. & Dixon, D. G. Chronic toxicity of waterborne thiocyanate to the fathead minnow (pimephales promelas): A partial life-cycle study. *Environ. Toxicol. Chem.* **13**, 1423–1432 (1994).
3. Lanno, R. P. & Dixon, D. G. Chronic toxicity of waterborne thiocyanate to rainbow trout (Oncorhynchus mykiss). *Can. J. Fish. Aquat. Sci.* **53**, 2137–2146 (1996).
4. Lanno, R. P. & Dixon, D. G. The comparative chronic toxicity of thiocyanate and cyanide to rainbow trout. *Aquat. Toxicol.* **36**, 177–187 (1996).
5. Logue, B. A., Hinkens, D. M., Baskin, S. I. & Rockwood, G. A. The analysis of cyanide and its breakdown products in biological samples. *Crit. Rev. Anal. Chem.* **40**, 122–147 (2010).
6. Okolie, N. P. & Osagie, A. U. Liver and kidney lesions and associated enzyme changes induced in rabbits by chronic cyanide exposure. *Food Chem. Toxicol.* **37**, 745–750 (1999).

7. Swenne, I. *et al.* Cyanide detoxification in rats exposed to acetonitrile and fed a low protein diet. *Fundam. Appl. Toxicol.* **32**, 66–71 (1996).
8. Rodkey, F. L. & Robertson, R. F. Analytical precautions in measurement of blood cyanide. *Clin. Chem.* **24**, 2184–2185 (1978).
9. Pettigrew, A. R. & Fell, G. S. Microdiffusion method for estimation of cyanide in whole blood and its application to the study of conversion of cyanide to thiocyanate. *Clin. Chem.* **19**, 466–471 (1973).
10. Sousa, A. B., Manzano, H., Soto-Blanco, B. & Górniak, S. L. Toxicokinetics of cyanide in rats, pigs and goats after oral dosing with potassium cyanide. *Arch. Toxicol.* **77**, 330–334 (2003).
11. Hasuike, Y. *et al.* Accumulation of cyanide and thiocyanate in haemodialysis patients. *Nephrol. Dial. Transplant.* **19**, 1474–1479 (2004).
12. Tsuge, K., Kataoka, M. & Seto, Y. Cyanide and thiocyanate levels in blood and saliva of healthy adult volunteers. *J. Heal. Sci.* **46**, 343–350 (2000).
13. Hall, A. H. & Borron, S. W. *Smoke Inhalation Toxicology of Cyanides and Cyanogens: Experimental, Applied and Clinical Aspects* (Wiley, 2016).
14. Goutam, M. P. & Yadav, P. Cyanide poisoning: Mass spectrometric analysis of forensic evidences. *Toxichem Krimtech* **87**, 103–116 (2020).
15. Karhunen, P. J., Lukkari, I. & Vuori, E. High cyanide level in a homicide victim burned after death: Evidence of post-mortem diffusion. *Forensic Sci. Int.* **49**, 179–183 (1991).
16. Petrikovics, I. *et al.* Organ-distribution of the metabolite 2-aminothiazoline-4-carboxylic acid in a rat model following cyanide exposure. *Biomarkers* **16**, 686–690 (2011).
17. McAllister, J. L., Roby, R. J., Levine, B. & Purser, D. Stability of cyanide in cadavers and in postmortem stored tissue specimens: A review. *J. Anal. Toxicol.* **32**, 612–620 (2008).
18. Hendry-Hofer, T. B. *et al.* A review on ingested cyanide: Risks, clinical presentation, diagnostics, and treatment challenges. *J. Med. Toxicol.* **15**, 128–133 (2019).
19. McAllister, J. L., Roby, R. J., Levine, B. & Purser, D. The effect of sodium fluoride on the stability of cyanide in postmortem blood samples from fire victims. *Forensic Sci. Int.* **209**, 29–33 (2011).
20. Mascini, M. Aptamers and their applications. *Anal. Bioanal. Chem.* **390**, 987–988 (2008).
21. Birch, J. R. & Racher, A. J. Antibody production. *Adv. Drug Deliv. Rev.* **58**, 671–685 (2006).
22. Ferreira, C. S. M. & Missailidis, S. Aptamer-based therapeutics and their potential in radiopharmaceutical design. *Braz. Arch. Biol. Technol.* **50**, 63–76 (2007).
23. Jayasena, S. D. Aptamers: An emerging class of molecules that rival antibodies in diagnostics. *Clin. Chem.* **45**, 1628–1650 (1999).
24. Ireson, C. R. & Kelland, L. R. Discovery and development of anticancer aptamers. *Mol. Cancer Ther.* **5**, 2957–2962 (2006).
25. Soares, S., Rosado, T., Barroso, M., Vieira, D. N. & Gallardo, E. Organophosphorus pesticide determination in biological specimens: Bioanalytical and toxicological aspects. *Int. J. Legal Med.* **133**, 1763–1784 (2019).
26. Gu, H. *et al.* Graphene oxide-assisted non-immobilized SELEX of okdaic acid aptamer and the analytical application of aptasensor. *Sci. Rep.* **6**, 1–9 (2016).
27. Thoa, T. T. T., Liao, A. M. & Thomas Caltagirone, G. Determining the thermodynamic and kinetic association of a DNA aptamer and tetracycline using isothermal titration calorimetry. *J. Vis. Exp.* **2022**, 1–8 (2022).
28. Wang, Y., Wang, G., Moitessier, N. & Mittermaier, A. K. Enzyme kinetics by isothermal titration calorimetry: Allostery, inhibition, and dynamics. *Front. Mol. Biosci.* **7**, 1–19 (2020).
29. Yadav, S. *et al.* An update on graphene oxide: Applications and toxicity. *ACS Omega* **7**, 35387–35445 (2022).
30. Shin, D. S. *et al.* Distribution of oxygen functional groups of graphene oxide obtained from low-temperature atomic layer deposition of titanium oxide. *RSC Adv.* **7**, 13979–13984 (2017).
31. Bart, J. *et al.* Room-temperature intermediate layer bonding for microfluidic devices. *Lab Chip* **9**, 3481–3488 (2009).
32. Lu, C. H., Yang, H. H., Zhu, C. L., Chen, X. & Chen, G. N. A graphene platform for sensing biomolecules. *Angew. Chemie - Int. Ed.* **48**, 4785–4787 (2009).
33. He, S. *et al.* A craphene nanoprobe for rapid, sensitive, and multicolor fluorescent DNA analysis. *Adv. Funct. Mater.* **20**, 453–459 (2010).
34. Ocaña, C. *et al.* Label free aptasensor for Lysozyme detection: A comparison of the analytical performance of two aptamers. *Bioelectrochemistry* **105**, 72–77 (2015).
35. Gillan, L., Teerinen, T., Johansson, L. S. & Smolander, M. Controlled diazonium electrodeposition towards a biosensor for C-reactive protein. *Sensors Int.* **2**, 100060 (2021).
36. Le, T. H., Pham, V. P., La, T. H., Phan, T. B. & Le, Q. H. Electrochemical aptasensor for detecting tetracycline in milk. *Adv. Nat. Sci. Nanosci. Nanotechnol.* **7**, 015008 (2016).
37. Aye, N. N. S. *et al.* Article a simple graphene functionalized electrochemical aptasensor for the sensitive and selective detection of glycated albumin. *Appl. Sci.* **11**, 10315 (2021).
38. Youn, H. *et al.* Aptasensor for multiplex detection of antibiotics based on FRET strategy combined with aptamer/graphene oxide complex. *Sci. Rep.* **9**, 1–9 (2019).
39. Logue, B. A. *et al.* Determination of the cyanide metabolite 2-aminothiazoline-4-carboxylic acid in urine and plasma by gas chromatography-mass spectrometry. *J Chromatogr. B Anal. Technol. Biomed. Life Sci.* **819**, 237–244 (2005).
40. Logue, B. A., Maserek, W. K., Rockwood, G. A., Keebaugh, M. W. & Baskin, S. I. The analysis of 2-amino-2-thiazoline-4-carboxylic acid in the plasma of smokers and non-smokers analysis of ATCA in smokers and non-smokers. *Toxicol. Mech. Methods* **19**, 202–208 (2009).
41. Giebułtowicz, J., Ruzycka, M., Fudalej, M., Krajewski, P. & Wroczyński, P. LC-MS/MS method development and validation for quantitative analyses of 2-aminothiazoline-4-carboxylic acid—A new cyanide exposure marker in post mortem blood. *Talanta* **150**, 586–592 (2016).
42. Baskin, S., Petrikovics, I., Platoff, G., Rockwood, G. & Logue, B. Spectrophotometric analysis of the cyanide metabolite 2-aminothiazoline-4- carboxylic acid (ATCA). *Toxicol. Mech. Methods* **16**, 339–345 (2006).
43. Jackson, R. & Logue, B. A. A review of rapid and field-portable analytical techniques for the diagnosis of cyanide exposure. *Anal. Chim. Acta* **960**, 18–39 (2017).
44. Ahmad Raston, N. H. & Gu, M. B. Highly amplified detection of visceral adipose tissue-derived serpin (vaspin) using a cognate aptamer duo. *Biosens. Bioelectron.* **70**, 261–267 (2015).
45. Lipfert, J., Doniach, S., Das, R. & Herschlag, D. Understanding nucleic acid-ion interactions. *Annu. Rev. Biochem.* **83**, 813–841 (2014).
46. Jackson, R., Petrikovics, I., Lai, E. P. C. & Yu, J. C. C. Molecularly imprinted polymer stir bar sorption extraction and electrospray ionization tandem mass spectrometry for determination of 2-aminothiazoline-4- carboxylic acid as a marker for cyanide exposure in forensic urine analysis. *Anal. Methods* **2**, 552–557 (2010).
47. Petrikovics, I. *et al.* Plasma persistence of 2-aminothiazoline-4-carboxylic acid in rat system determined by liquid chromatography tandem mass spectrometry. *J Chromatogr. B Anal. Technol. Biomed. Life Sci.* **891–892**, 81–84 (2012).
48. Luliński, P., Giebułtowicz, J., Wroczyński, P. & Maciejewska, D. A highly selective molecularly imprinted sorbent for extraction of 2-aminothiazoline-4-carboxylic acid—Synthesis, characterization and application in post-mortem whole blood analysis. *J. Chromatogr. A* **1420**, 16–25 (2015).

49. Giebułtowicz, J., Sobiech, M., Rużycka, M. & Luliński, P. Theoretical and experimental approach to hydrophilic interaction dispersive solid-phase extraction of 2-aminothiazoline-4-carboxylic acid from human post-mortem blood. *J. Chromatogr. A* **1587**, 61–72 (2019).
50. Li, S. *et al.* Development of magnetic carbon nanotubes for dispersive micro solid phase extraction of the cyanide metabolite, 2-aminothiazoline-4-carboxylic acid, in biological samples. *J Chromatogr. B Anal. Technol. Biomed. Life Sci.* **1109**, 67–75 (2019).
51. Hisatsune, K. *et al.* RECiQ: A rapid and easy method for determining cyanide intoxication by cyanide and 2-aminothiazoline-4-carboxylic acid quantification in the human blood using probe electrospray ionization tandem mass spectrometry. *ACS Omega* **5**, 23351–23357 (2020).

Acknowledgements

H.M.A. Khan received a scholarship from the Malaysian Public Service Department (PSD). The authors would like to thank Mr. Azharuddin bin Abdul Aziz (Department of Chemistry Malaysia) and Mrs. Hazalinawati binti Zailani (Department of Chemistry Malaysia, Sarawak State) for their technical and theoretical support.

Author contributions

H.M.A. Khan: conceptualization, methodology, formal analysis, writing—original draft preparation; N.A. Yusof: project administration, supervision, writing—review and editing; S.A.A. Ahmad: supervision; C.Y. Yu: validation, supervision; N.H.A. Raston: supervision; S.F.A. Rahman: writing—review and editing. All authors reviewed the manuscript.

Competing interests

The authors declare no competing interests.

Additional information

Correspondence and requests for materials should be addressed to N.A.Y. or S.F.A.R.